Cerebellum (2013) 12:406–417
DOI 10.1007/s12311-012-0429-8

ORIGINAL PAPER

Principal Component and Cluster Analysis of Morphological Variables Reveals Multiple Discrete Sub-phenotypes in *Weaver* Mouse Mutants

Joaquín Martí · María C. Santa-Cruz · Roger Serra · Oliver Valero · Vanessa Molina · José P. Hervás · Sandra Villegas

Published online: 24 November 2012

Abstract The present study evaluates the usefulness of the principal component analysis-based cluster analysis in the categorization of several sub-phenotypes in the *weaver* mutant by using several morphological parameters from the cerebellar cortex of control, heterozygous (+/*wv*) and homozygous (*wv*/*wv*) *weaver* mice. The quantified parameters were length of the cerebellar cortex, area of the external granular layer, area of the molecular layer, number of the external granular layer cells (EGL), and number of Purkinje cells (PCs). The analysis indicated that at postnatal day 8, the genotype +/*wv* presented three sub-phenotypes tagged as +/wv^0, +/wv^1 and +/wv^2, whereas two sub-phenotypes designated as wv^0/wv^1 and wv^0/wv^2 were identified in the genotype *wv*/*wv*. The number of PCs for the genotype +/*wv* and the number of EGL cells for the genotype *wv*/*wv* were the variables that discriminated the best among sub-phenotypes. Each one of the sub-phenotypes showed specific abnormalities in the cytoarchitecture of the cerebellar cortex as well as in the foliar pattern. In particular, the wv^0/wv^1 and wv^0/wv^2 sub-phenotypes had the most altered cytoarchitectonics, followed by the +/wv^2 sub-phenotype and then by the +/wv^1 one. The sub-phenotype +/wv^0 was the less affected one. Apart from reporting for the first time the coexistence of several sub-phenotypes in the *weaver* mutant, our approach provides a new statistical tool that can be used to assess cerebellar morphology.

Keywords Heterozygous *weaver* · Homozygous *weaver* · PCA-based cluster analysis · Foliar pattern · External granular layer · Purkinje cells

Introduction

The mammalian cerebellum is a foliated structure formed of a central vermis and two bilaterally symmetric hemispheres, each with its own sets of fissures [1]. The cerebellum has a regular cytoarchitecture composed by two discrete components: the cerebellar cortex in a superficial position and, buried, an aggregate of neurons that constitutes the deep cerebellar nuclei [2]. The adult cerebellar cortex exhibits three layers. First, the molecular layer located the under the pial membrane comprises two main types of interneurons, the basket and the stellate cells. The Purkinje cell layer contains the cell bodies of Purkinje cells (PCs) whose dendrites arborize in the molecular layer (ML). They are the sole output neuron of the cerebellar cortex, via connections with neurons in the cerebellar nuclei [3], which project efferent fibers to the thalamus, brainstem, and spinal cord [4, 5]. The deepest layer, the granule cell layer, presents the cell bodies of the granule cells (GCs) and other interneurons such as Golgi, Lugaro, candelabrum and unipolar brush cells [6, 7].

Studies using chick–quail chimeras showed that the cerebellum derives from the region of the neural tube, which encompasses the caudal portion of the mesencephalic

J. Martí (✉) · M. C. Santa-Cruz · R. Serra · V. Molina · J. P. Hervás
Departament de Biologia Cel.lular, de Fisiologia i d'Immunologia. Unidad de Citologia i d'Histologia. Facultat de Biociències, Universitat Autònoma de Barcelona, 08193 Bellaterra, Barcelona, Spain
e-mail: Joaquim.Marti.Clua@uab.cat

O. Valero
Servei d'Estadística Aplicada, Universitat Autònoma de Barcelona, 08193 Bellaterra, Barcelona, Spain

S. Villegas (✉)
Departament de Bioquímica i Biologia Molecular. Facultat de Biociències, Universitat Autònoma de Barcelona, 08193 Bellaterra, Barcelona, Spain
e-mail: sandra.villegas@uab.cat

vesicle and the rostral portion of the metencephalic vesicle [8]. Subsequent gene expression and fate mapping analysis indicated that this region of the CNS arises entirely from the anterior-most rhombomere of the hindbrain, rhombomere 1 [9, 10]. Over this period, it was also seen that the isthmus, the neural tissue at the metencephalic–mesencephalic junction, plays an important role in the establishment of the cerebellar territory [8]. It is accepted that the organizing activity of the isthmic tissue is mediated by the secreted fibroblast growth factor 8 [10, 11].

The establishment of the cerebellar territory is followed by the formation of two germinative compartments, the ventricular neuroepithelium and the anterior rhombic lip. All cerebellar neurons derive from the above regions according to a well-defined spatiotemporal sequence [1]. GABAergic neurons, such as Purkinje cells and inhibitory interneurons, are generated from the ventricular neuroepithelium upon pancreas transcription factor 1a control. By contrast, glutamatergic neurons, including deep cerebellar nuclei neurons, unipolar brush cells and GCs derive from Math-1-expressing progenitors that emigrate from the rhombic lip [12, 13].

There are several mutations that affect the development of the cerebellum (http://www.informatics.jax.org/). One of these is the *weaver* mutation (*Kcnj6* gene), located on mouse chromosome 16 [14, 15]. Its genetic basis consists of a single base-pair substitution that generates a missense mutation (Ser156Gly) affecting the highly conserved H5 domain of the inwardly rectifying GIRK2, a G-protein coupled K^+ channel [16].

Homozygous *weaver* mice (*wv*/*wv*) have been proposed as model for Parkinson's disease [17, 18] and cerebellar ataxia [19] because they present motor abnormalities [20]. These impairments arise as a consequence of the extensive loss of dopaminergic neurons in the midbrain [21, 22] and of GCs, PCs and deep cerebellar nuclei neurons in the cerebellum [23–29]. In the heterozygous *weaver* mice (+/*wv*), on the other hand, the depletion of neurons seems to be less evident [23, 24, 26, 27, 30] and they do not present behavioral abnormalities [23, 31].

Previous studies have demonstrated that, in the *wv*/*wv* cerebellar cortex, the depletion of GCs and PCs occurs according to a lateral-to-medial gradient of increasing severity [24–27, 29, 32]; the vermis is the most severely affected region, while in the hemispheres the neuronal deficit is spared. This, together with the ectopic location of the surviving GCs and PCs [24, 25, 28, 33], determine important regional differences in the cytoarchitecture of the vermal region [27, 32, 34].

The aim of this paper is to show that the use of several morphological parameters from the cerebellar cortex of control, heterozygous, and homozygous *weaver* mice in a principal component analysis (PCA)-based cluster analysis [35–38] could be useful to assess cerebellar morphology, as well as to illustrate that these sub-phenotypes exhibit different cytoarchitectonics and foliar pattern.

Materials and Methods

Animals

All mice used in this study were obtained from the colony of control and homozygous *weaver* mice at Indiana University School of Medicine maintained on the B6CBA-$A^{w\text{-}j}$/A hybrid stock. The parents of the +/+, +/*wv* and *wv*/*wv* offspring used in the present study were either +/*wv* or *wv*/*wv* females mated to +/*wv* males. It is worth mentioning that this paper is included in a series which analyzes the development of the +/*wv* and *wv*/*wv* central nervous system. The animal subjects included in the present work were also used in a [^{3}H]TdR autoradiography study to get insight in the generation and settling of +/*wv* and *wv*/*wv* EGL cells and Purkinje neurons [39]. Thus, we have used the series injected at embryonic days E14–15, time at which PC neurogenesis is almost completed, and the label is just residually incorporated. Signs of toxicity were never observed and cerebella of the injected animals appeared normal in both size and cell number.

The mice were maintained in controlled environment (lights on from 07:30 to 19:30 hours; temperature, 22± 2 °C). They had free access to food and water. A total of 54 mice were processed for histology at P8. All procedures were approved by the animal care and use committee of our university.

Wv mutation consists of a point mutation in the GIRK2 gene, and was ascertained by means of SSCP (single-strand conformational polymorphism) [40]. Genotypes were also confirmed by microscopic examination of the cerebellum, which is smaller and has disorganized cytoarchitecture as a consequence of the depletion of several neuron populations [24].

Perfusion and Histology

At P8, animals were deeply anesthetized with sodium pentobarbital (50 mg/kg i.p.) and perfused through the heart with 4 % paraformaldehyde in phosphate-buffered saline (pH 7.4). Brains were removed, dissected, and post-fixed for 5 h at 4 °C. Next, they were dehydrated in graded-ethanol solutions prior to being embedded in paraffin. In order to avoid overestimation of cell counts, the block containing the cerebellum was sectioned serially at 10 μm in the sagittal plane and one of every six sections was placed on poly-(L-lysine)-coated slides. Care was taken to keep the long axis of the brain parallel to the side of the block and the bottom of both cerebral hemispheres touching the base

of the embedding box, to avoid tilting of the cerebellum so as to obtain true sagittal sections. Only those sections representative of the medial point of the vermis were used in the present study. Sections were stained using two procedures: haematoxylin or cresyl violet.

Morphometry of the Cerebellum

The following features of the cerebellar morphology were quantified per section: length of the cerebellar cortex, area of the EGL, area of the ML, number of EGL cells, and number of PCs. Each parameter was determined in three sections of every experimental animal. Data from each section were added to obtain a mean for each cerebellar feature per mouse. Under identical lighting conditions, images of sectioned cerebella were captured by a CCD-IRIS color video camera (Sony, Japan) coupled to a Zeiss Axiosphot microscope and digitalized. Morphometric analysis was performed with the Visilog 5 software (Noesis, France). Analysis was done as follows: the first step was calibration to convert pixel units to metric units. Subsequently, length of the cerebellar cortex, as well as EGL and ML areas, were delimited manually to obtain initial binary images. Images of total cerebellum, entire EGL and entire ML were submitted to the mentioned software to obtain the length of the cerebellar cortex, area of the EGL and area of the ML.

Counts of EGL cells and PCs were carried out in the pertinent sections by visual scanning of the cerebellar cortex throughout the entire anteroposterior profile. The amount of EGL cells was determined using a 1,000× oil immersion objective and an ocular graticule. Criteria for scoring them included both morphological and staining properties. Small, darkly stained and densely packed cells, most of them round-like in shape were considered as EGL cells. Pyknotic nuclei and endothelial cells were easily discerned. On the other hand, PCs were counted on the bases of several assumptions such as size, the morphological characteristics of the pericarion and distinctive stain properties. These macroneurons were counted at 400×, and considered as present if they possessed large pyriform somata and nucleus with the presence of a distinct nucleolus. Since *wv*/*wv* PCs somata are ectopically settled due to disruption of the normal cerebellar cortex cytoarchitecture [27, 32, 34], it may be difficult to distinguish between PCs and any other large neurons in our sections. Total PC counts in the *wv*/*wv* were therefore multiplied by a Golgi cell correction factor (85.7 %). This correction factor was derived from the PCs/Golgi cell ratio in lower mammals [41] and it was previously used in quantitative analyses of *weaver* PCs [26, 42].

Qualitative Analyses of the Cerebellar Cortex

Light microscopic analyses of cerebellum were made with a Zeiss Axiosphot microscope using a wide set of objectives. Observations were focused at the superficial (convex) areas of the following lobules. From the anterior lobe, the lobules lingula, culmen and centralis were examined; the tuber and the pyramis from the central lobe; the uvula from the posterior and the nodulus from the inferior lobe. The deep of the prima, secunda and posterolateralis fissures were also studied. The names of the lobes and lobules used in this paper are those previously assigned by Altman and Bayer [1].

Statistical Analysis

Means±the standard error of the means were obtained for each quantified parameter of the cerebellar morphology. Pearson correlation coefficient for each pair of variables was computed. To reduce the dimensionality of the variables' set, a PCA was performed [36]. The new components obtained from the PCA were submitted to a cluster analysis applying the Ward's Hierarchical Clustering Method [35, 37]. The cubic clustering criterion [43] was used to determine the optimum number of clusters and R^2 distance was used to represent the clusters in a tree dendogram [44].

The accuracy of the classification was evaluated by performing a leave on out cross-validation. The description and comparison of the clusters was analyzed by bivariate analysis of variance; post hoc pair-wise comparisons were carried out using Student–Newman–Keuls method. Additionally, a canonical discriminant analysis [36] was performed to find linear combinations of morphological parameters providing maximal separation among clusters. Total sample standardized canonical coefficients and scatter plots are presented.

The statistical analysis has been performed using software SAS v9.2 (SAS Institute Inc., Cary, NC, USA). P values lower than 0.05 were considered statistically significant.

Results

Assigning Genotypes and Phenotypes

Animals were assigned to one of the three genotypes: wild type (+/+; n=15), +/*wv* (n=28) and *wv*/*wv* (n=11). Assignation was first based on light microscopic criteria in accordance with previous descriptions [24, 25, 45, 46] and then confirmed by SSCP [40].

Quantified parameters of the cerebellar morphology for each genotype are summarized in Table 1. Pearson correlation coefficient for each pair of variables was computed and a correlation matrix was generated (Table 2). Because these variables are highly correlated, a PCA was performed to reduce the number of variables before applying cluster analysis. All variables were standardized such that each variable

was given the same weight in the PCA. The first two principal components accounted for 98 % of the total variance (Fig. 1). The first and most important component is an average measure of all variables since all of them show approximately equal loadings. The second component has high positive loadings on the length of the cerebellar cortex and a negative weight on the EGL cell number.

A cluster analysis was applied to these two principal components in order to classify heterozygous and homozygous *weaver* mice into potential sub-phenotypes. The cubic clustering criterion indicated that the optimum number of clusters was 5. All controls were classified into cluster 1, heterozygous were categorized into three clusters [2–4], whereas homozygous were initially cataloged into cluster 5 (Fig. 2a). Heterozygous sub-phenotypes were tagged as $+/wv^0$ (n=15), $+/wv^1$ (n=7) and $+/wv^2$ (n=6).

Because many homozygous *weaver* mice died early, typically before adulthood (personal observation) and much of them are sterile [47, 48], it became difficult to obtain a large group of animals. In consequence, the low number of homozygous animals used in this study (n=11) could preclude initial classification into clusters and a second analysis was performed considering only this group. Two clusters were then found (5A and 5B, Fig. 2b), designated as wv^0/wv^1 (n=6) and wv^0/wv^2 (n=5).

The accuracy in the subsequent leave on out cross-validation of the nested cluster analysis was 100 %. Results from the bivariate analysis of variance and individual data points of each quantified cerebellar feature for all sub-phenotypes are shown in Tables 3, 4, 5, 6, and 7. These analyses revealed that all of the analyzed features vary in accordance to the described sub-phenotypes. These parameters are larger in the +/+, smaller in sub-phenotypes $+/wv^0$, $+/wv^1$ and $+/wv^2$ and smallest in sub-phenotypes wv^0/wv^1 and wv^0/wv^2. When the $+/wv$ sub-phenotypes were separately considered, it was observed that values were greatest in the $+/wv^0$, less in the $+/wv^1$, and least in the $+/wv^2$. Except for the length of the cerebellar cortex, the remainder analyzed parameters were larger in the wv^0/wv^1 than in the wv^0/wv^2 sub-phenotype.

In order to determine which features discriminated the best among clusters, a canonical discriminant analysis was performed. From this analysis, we obtained linear combinations of the variables providing maximal separation among clusters (Fig. 3a and b). The first canonical variable explains more than 95 % of the total variation and the two canonical variables extracted explain the 100 %. Table 8 presents the standardized coefficients for the canonical variables. The number of PCs is the variable which most contributes to the discrimination

Table 1 Mean±SEM of the quantified features of the cerebellar morphology for each genotype

Features	Genotype	Mean	SEM
Cerebellar cortex length per section	+/+	30.15	0.7
Cerebellar cortex length per section	*+/wv*	19.46	0.9
Cerebellar cortex length per section	*wv/wv*	8.18	0.5
External granular layer area per section	+/+	689.73	17.7
External granular layer area per section	*+/wv*	428.56	17. 3
External granular layer area per section	*wv/wv*	173.76	11.3
Molecular area per section	+/+	1066.4	28.1
Molecular area per section	*+/wv*	628.68	38.9
Molecular area per section	*wv/wv*	45.35	6.3
External granular layer cells per section	+/+	21.57	0.6
External granular layer cells per section	*+/wv*	13.25	0.6
External granular layer cells per section	*wv/wv*	5.57	0.4
Purkinje cells number per section	+/+	635.20	7.3
Purkinje cells number per section	*+/wv*	436.43	17.3
Purkinje cells number per section	*wv/wv*	172.55	7.2

Values for the cerebellar cortex length per section are expressed in millimeters. Those for the external granular and molecular layers areas per section are expressed in $\times 10^{-3}$ μm^2. Finally, data for the number of external granular layer cells per section are represented as $\times 10^{-3}$

Table 2 Matrix of Pearson correlation coefficient for each pair of variables

	Correlation matrix				
	Length CC	EGL area	ML area	EGL cells	PCs
Length CC	1.0000	0.9457	0.9546	0.9344	0.9565
EGL area	0.9457	1.0000	0.9607	0.9665	0.9670
ML area	0.9546	0.9607	1.0000	0.9648	0.9871
EGL cells	0.9344	0.9665	0.9648	1.0000	0.9742
PCs	0.9565	0.9670	0.9871	0.9742	1.0000

Note that all of them are highly correlated

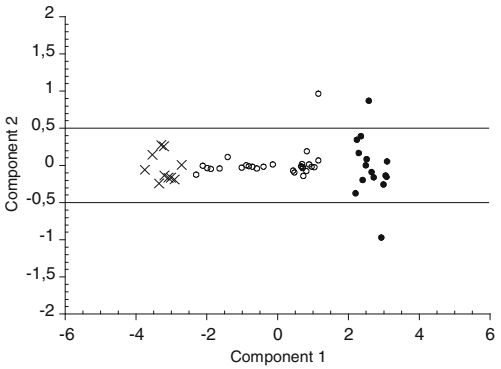

Fig. 1 Principal components analysis. Position of wild-type (*filled circle*), heterozygous *weaver* (*empty circle*) and homozygous *weaver* (*multiplication symbol*) in the plane spanned by the first two principal components. The area delimited by two lines represents the 95 % confidence interval for the two principal components. The first and most important component is an average measure of all variables since all of them show approximately equal loadings. The second component has high positive loadings on the length of the cerebellar cortex and a negative weight on the EGL cell number

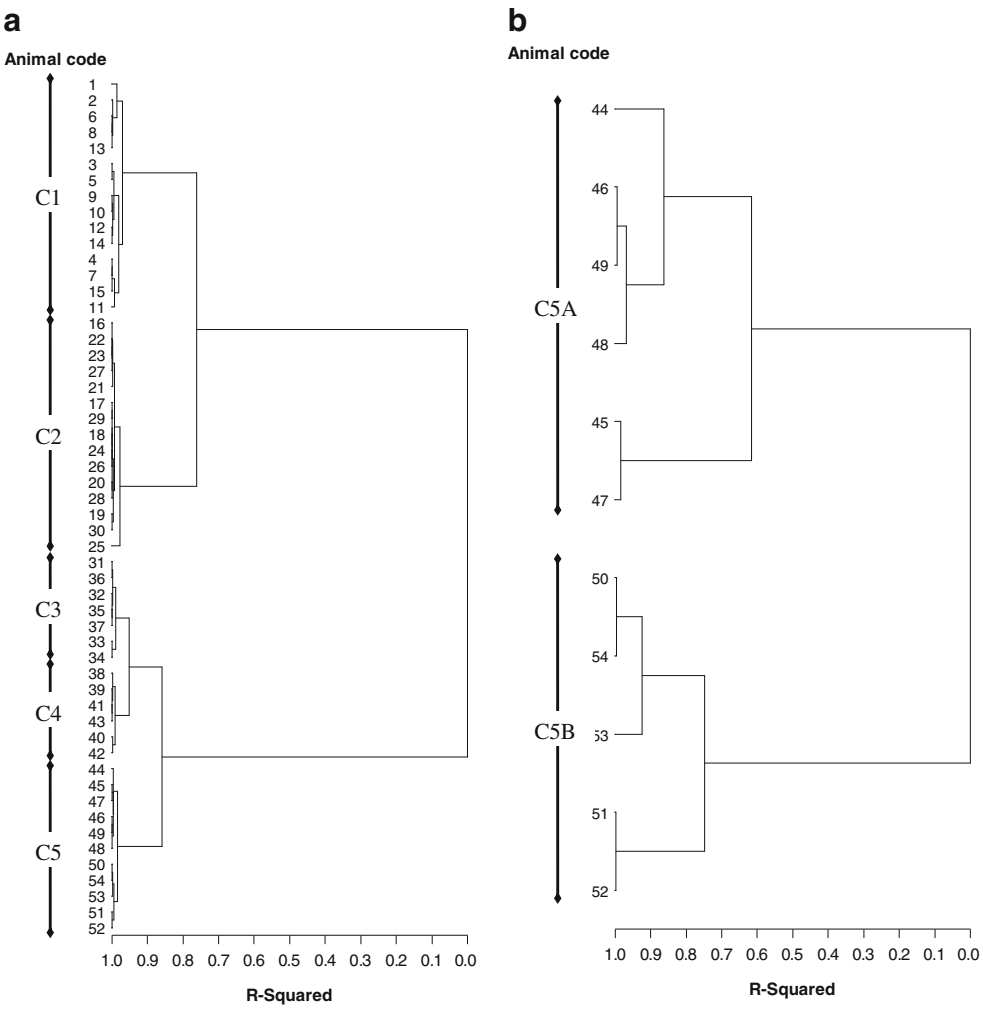

Fig. 2 Cluster analysis. Dendogram showing PCA-based cluster analysis results for all of the quantified parameters. *Arrows* at the side of each tree branch delineate the clusters. **a** Initial clustering. **b** Clustering applied to data from homozygous *wv*/*wv* animals alone

among the initial clusters, whereas for the further clustering of homozygous animals the number of EGL cells was the one which most contributed to the discrimination between the two clusters found.

Qualitative Observations in the Cerebellar Cortex

Vermal sagittal sections from each sub-phenotype illustrating the lobular organization of the cerebellar cortex are shown in Fig. 4. It is observed that in each sub-phenotype the cerebellum appears as a folded structure with a pattern of creases and fissures relatively well developed. Despite, compared to the wild-type, foliar size was smaller in the $+/wv^0$, $+/wv^1$ and $+/wv^2$ ones and smallest in the wv^0/wv^1 and wv^0/wv^2 ones. Those fissures that determine the limits between the cerebellar cortex lobes (prima, secunda and posterolateralis) were present in each sub-phenotype at which identification of the cerebellar lobes and lobules was reliable.

A closer analysis reveals that the +/+ cerebellar cortex exhibits its characteristic trilaminar disposition throughout. Briefly, it presents a subpial structure, the EGL, being formed by small, darkly stained and densely packed cells, most of which are round-like in shape. Immediately beneath the EGL is the ML, which contains basket and stellate cells as well as vertically oriented spindle-shaped cells (the differentiating granule cells). Next, the Purkinje cell layer, composed of large somata of PCs arranged in a single and straight row, is found. Finally, the internal granular layer is formed of very densely-packed somata of small neurons; the GCs.

In contrast, two unusual features are seen in the cerebellar cortex of heterozygous *weaver* mice. Thus, in the $+/wv^0$ sub-phenotype PCs are placed in a quasimonolayer in each studied region. This arrangement changed in the sub-phenotypes $+/wv^1$ and $+/wv^2$, as the number of strata in which these macroneurons are distributed varied from area to area in both sub-phenotypes (Table 9). Another difference recognized by light microscopy was the presence, in the ML of the $+/wv^1$ and $+/wv^2$ sub-phenotypes, of a distinctive band of darkly stained cells, whose density depends on both the sub-phenotype and the studied area (Table 9). Band showing an increased density of cells in the ML was not observed in the $+/wv^0$ sub-phenotype or in the +/+ one. Figure 5 exhibits both unusual

Table 3 Individual data points for the cerebellar cortex length per section in the phenotypes noted in this work

+/+	$+/wv^0$	$+/wv^1$	$+/wv^2$	wv^0/wv^1	wv^0/wv^2
25.7 (1)	25.6 (16)	17.4 (31)	10.3 (38)	10.7 (44)	7.9 (50)
32.8 (2)	21.9 (17)	15.8 (32)	11.9 (39)	5.9 (45)	10.1 (51)
26.5 (3)	22.3 (18)	19.3 (33)	15.8 (40)	7.7 (46)	10.4 (52)
30.3 (4)	20.7 (19)	18.1 (34)	12.4 (41)	7.4 (47)	5.4 (53)
26.9 (5)	21.3 (20)	16.8 (35)	13.5 (42)	8.2 (48)	8.3 (54)
30.5 (6)	24.2 (21)	17.1 (36)	12.1 (43)	8.0 (49)	
32.1 (7)	23.5 (22)	16.6 (37)			
30.7 (8)	23.8 (23)				
29,0 (9)	22.1 (24)				
31.3 (10)	31.8 (25)				
37.0 (11)	22,0 (26)				
29.8 (12)	23.4 (27)				
29.6 (13)	22.5 (28)				
30.1 (14)	22.2 (29)				
30.0 (15)	20.5 (30)				
30.2±0.7 a	23.2±0.7 b	17.3±0.4 c	12.7±0.8 d	8.0±0.7 e	8.4±0.9 e

Values are expressed in millimeters. Number in parenthesis refers to animal code. Groups with different letters differ statistically. Student–Newman–Keuls test ($p<0.05$)

Shadowed row indicates means±SEM. One-way ANOVA, $F(5, 48)=131.67$ ($P<0.001$)

Table 4 Individual data points for the external granular layer area per section in the phenotypes noted in this work

+/+	$+/wv^0$	$+/wv^1$	$+/wv^2$	wv^0/wv^1	wv^0/wv^2
680 (1)	541 (16)	401 (31)	268 (38)	234 (44)	129 (50)
702 (2)	492 (17)	325 (32)	279 (39)	169 (45)	157 (51)
731 (3)	497 (18)	470 (33)	306 (40)	199 (46)	161 (52)
600 (4)	485 (19)	410 (34)	301 (41)	175 (47)	113 (53)
615 (5)	500 (20)	351 (35)	332 (42)	220 (48)	151 (54)
743 (6)	526 (21)	375 (36)	291 (43)	204 (49)	
667 (7)	512 (22)	340 (37)			
704 (8)	523 (23)				
678 (9)	499 (24)				
579 (10)	497 (25)				
648 (11)	508 (26)				
767 (12)	507 (27)				
801 (13)	506 (28)				
800 (14)	480 (29)				
631 (15)	478 (30)				
689.7± 17.7 a	503.4± 4.4 b	381.7± 19.2 c	296.2± 9.3 d	200.2± 10.5 e	142.2± 9.3 f

Values are expressed as $\times 10^{-3}$ μm^2. Number in parenthesis refers to animal code. Groups with different letters differ statistically. Student–Newman–Keuls test ($p<0.05$)

Shadowed row indicates means±SEM. One-way ANOVA, $F(5, 48)=197.7$ ($P<0.001$)

Table 5 Individual data points for the molecular layer area per section in the phenotypes noted in this work

+/+	$+/wv^0$	$+/wv^1$	$+/wv^2$	wv^0/wv^1	wv^0/wv^2
1050 (1)	840 (16)	528 (31)	248 (38)	80 (44)	37 (50)
1173 (2)	789 (17)	478 (32)	271 (39)	45 (45)	29 (51)
0879 (3)	795 (18)	647 (33)	390 (40)	54 (46)	25 (52)
1078 (4)	785 (19)	583 (34)	309 (41)	49 (47)	23 (53)
1236 (5)	801 (20)	510 (35)	335 (42)	72 (48)	21 (54)
1178 (6)	783 (21)	512 (36)	297 (43)	65 (49)	
0999 (7)	817 (22)	499 (37)			
1201 (8)	818 (23)				
1078 (9)	799 (24)				
1006 (10)	783 (25)				
0998 (11)	795 (26)				
0977 (12)	816 (27)				
1201 (13)	807 (28)				
0927 (14)	784 (29)				
1015 (15)	784 (30)				
1,066.4± 28.1 a	799.7± 4.3 b	536.7± 22.5 c	308.3± 20.9 d	60.8± 5.8 e	27.0± 2.9 f

Values are expressed as $\times 10^{-3}$ μm^2. Number in parenthesis refers to animal code. Groups with different letters differ statistically. Student–Newman–Keuls test ($p<0.05$)

Shadowed row indicates means±SEM. One-way ANOVA, $F(5, 48)=361.01$ ($P<0.001$)

Table 6 Individual data points for the number of external granular layer cells per section in the phenotypes noted in this work

+/+	$+/wv^0$	$+/wv^1$	$+/wv^2$	wv^0/wv^1	wv^0/wv^2
27.7 (1)	18.1 (16)	12.1 (31)	07.5 (38)	7.3 (44)	4.1 (50)
23.5 (2)	15.1 (17)	11.3 (32)	07.7 (39)	5.7 (45)	4.7 (51)
21.2 (3)	15.1 (18)	12.7 (33)	10.3 (40)	6.4 (46)	5.2 (52)
18.3 (4)	14.7 (19)	12.4 (34)	08.4 (41)	6.1 (47)	3.9 (53)
20.8 (5)	15.8 (20)	11.8 (35)	09.1 (42)	6.9 (48)	4.3 (54)
22.5 (6)	14.9 (21)	11.9 (36)	08.1 (43)	6.7 (49)	
19.3 (7)	16.7 (22)	11.6 (37)			
23.1 (8)	17,0 (23)				
19.8 (9)	15.3 (24)				
23.1 (10)	14.9 (25)				
19.6 (11)	15.1 (26)				
21.7 (12)	16.4 (27)				
22.3 (13)	16.5 (28)				
20.8 (14)	15.9 (29)				
19.9 (15)	14.7 (30)				
21.6±0.6 a	15.7±0.3 b	11.9±0.2 c	8.5±0.4 d	6.5±0.3 e	4.4±0.2 f

Values are expressed as $\times 10^{-3}$. Number in parenthesis refers to animal code. Groups with different letters differ statistically. Student–Newman–Keuls test ($p<0.05$)

Shadowed row indicates means±SEM. One-way ANOVA, $F(5, 48)=186.9$ ($P<0.001$)

Table 7 Individual data points for the Purkinje cell number per section in the phenotypes noted in this work

+/+	$+/wv^0$	$+/wv^1$	$+/wv^2$	wv^0/wv^1	wv^0/wv^2
680 (1)	484 (16)	406 (31)	261 (38)	205 (44)	143 (50)
642 (2)	538 (17)	386 (32)	274 (39)	174 (45)	157 (51)
598 (3)	514 (18)	415 (33)	317 (40)	189 (46)	165 (52)
643 (4)	477 (19)	426 (34)	294 (41)	182 (47)	138 (53)
621 (5)	521 (20)	394 (35)	311 (42)	204 (48)	149 (54)
676 (6)	514 (21)	399 (36)	286 (43)	192 (49)	
598 (7)	529 (22)	390 (37)			
670 (8)	531 (23)				
658 (9)	499 (24)				
647 (10)	511 (25)				
599 (11)	503 (26)				
638 (12)	515 (27)				
601 (13)	507 (28)				
630 (14)	516 (29)				
627 (15)	502 (30)				
635.2± 7.3 a	510.7± 4.2 b	402.3± 5.5 c	290.5± 8.9 d	191.0± 5.1 e	150.4± 4.9 f

Number in parenthesis refers to animal code. Groups with different letters differ statistically. Student–Newman–Keuls test ($p<0.05$)

Shadowed row indicates means± SEM. One-way ANOVA, $F(5, 48)=769.3$ ($P<0.001$)

features in the fissure prima and in the uvula of the sub-phenotype $+/wv^1$.

When the observations were focused on the *weaver* homozygotes, it was found that the cerebellar cortex does not exhibit the typical layering in any of the studied areas. The cytoarchitectonic disorder was conspicuous, which is in line with previous reports [27, 32]. This is because the PCs somas are dispersed in several irregular rows, which occupy most of the cortical area with the exception of the EGL and of a small ML. Moreover, the internal granular layer is not present, and GCs are scattered. The EGL, on the other hand, was found throughout the cerebellar cortex. A detailed examination focused in the anterior lobe of the wv^0/wv^2 sub-phenotype revealed that a lot of GCs degenerated within the EGL and completely disappeared. This degeneration was greatest in the culmen, lesser in the centralis and least in the lingula (see Fig. 6 and compare to Table 10).

Table 8 Total sample standardized canonical coefficients for the cluster analyses

Variable	Initial clustering		Clustering of homozygous	
	Canonical 1	Canonical 2	Canonical 1	Canonical 2
Lenght of the CC	1.008	−1.384	−2.173	0.847
EGL area/section	1.060	−1.651	0.562	−5.896
ML area/section	1.984	−1.470	−0.158	−0.740
EGL cells/section	−0.817	−3.879	7.253	−5.498
PCs/section	5.941	5.269	−2.380	10.372

Discussion

The results of this study confirm and extend previous data [27, 32, 34]; namely, that there are important regional differences in *weaver* gene action on the cortical architecture. Moreover, we also show here that these differences determine the existence of several sub-phenotypes in the *weaver* mutant mouse, showing each one of them impairments both in the cytoarchitectonics of the cerebellar cortical layers and in the foliar pattern. To our knowledge, this is the first time that the aforementioned sub-phenotypes are reported.

A point deserving attention when the sub-phenotypes are considered is whether the differences found both in the parameters quantified as well as the qualitative observations may be due to technical reasons such as mating protocol,

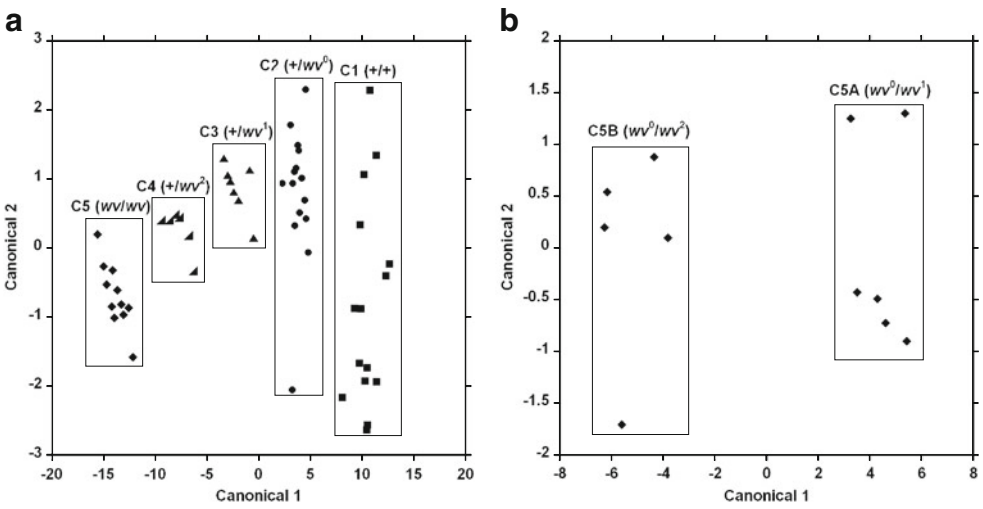

Fig. 3 Canonical discriminant analysis providing maximal separation among clusters. **a** Five clusters of mice are well differentiated in the initial clustering. **b** Two clusters of mice are well differentiated in the isolated clustering of homozygous animals

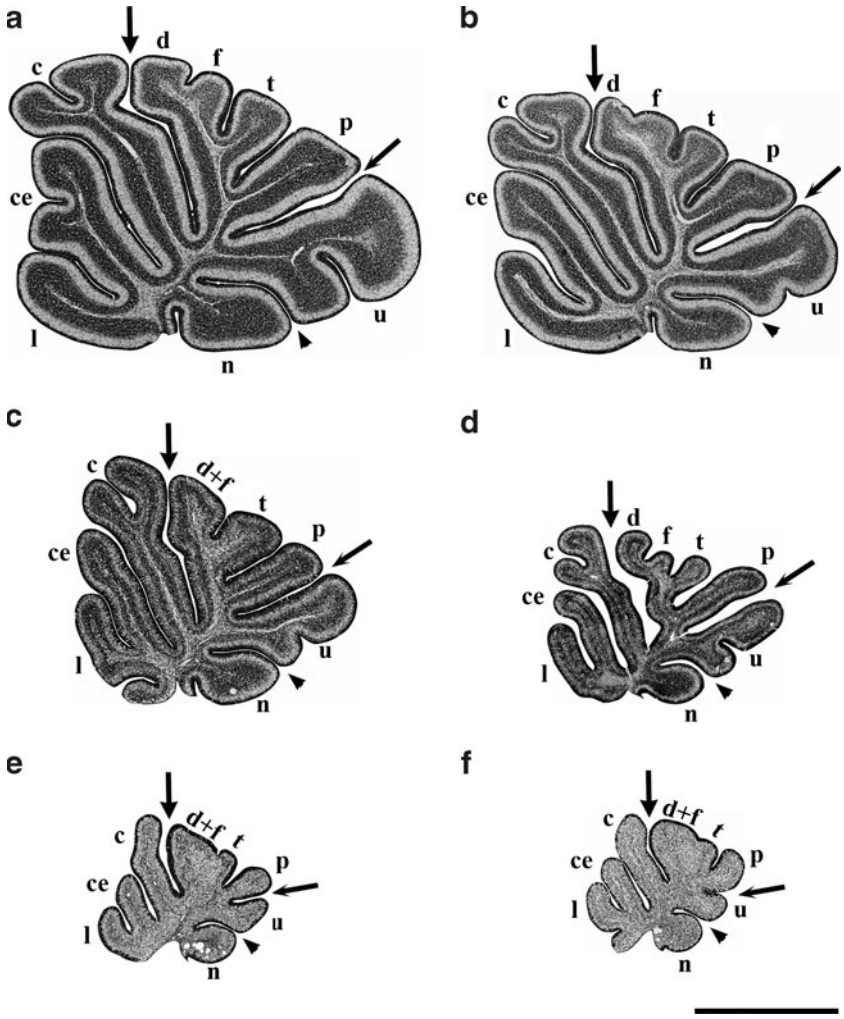

Fig. 4 Low magnification photomicrographs of the sagittally sectioned cerebellar vermis from wild type (**a**), heterozygous *weaver* (**b**–**d**) and homozygous *weaver* (**e**–**f**). Photomicrographs **b**, **c**, and **d** correspond to sub-phenotypes $+/wv^0$, $+/wv^1$ and $+/wv^2$, respectively, while those lettered **e** and **f** refer to sub-phenotypes wv^0/wv^1 and wv^0/wv^2, respectively. The anterior lobe ranges from the rostral pole of the cerebellar cortex to the fissure prima (long-stemmed arrow), the central lobe between the fissura prima and the fissura secunda (short-stemmed arrow), the posterior lobe between the secunda and the posterolateralis (*arrowhead*), and the inferior lobe. Vermal lobules are indicated as follows: *l* lingula, *ce* centralis, *c* culmen, *d* declive, *f* folium, *t* tuber, *p* pyramis, *u* uvula and *n* nodulus. *Scale bar* 1 mm

exact age of the mice or laboratory procedures. This seems unlikely, as the cerebellar alterations were individually and consistently observed in each sub-phenotype.

In order to obtain even more reliable data connecting the five sub-phenotypes clustered by the presented PCA to regional differences in the cytoarchitecture of their cerebellar cortex, more variables could be considered. Among them, those reflecting differences in the rostrocaudal (ratio of EGL thickness o PCs number among lobes o lobules) or lateromedial axes (rate between the length of the cerebellar cortex or ML area in the vermis *vs* hemispheres) could be used.

The present qualitative observations show that the ML of $+/wv^1$ and $+/wv^2$ sub-phenotypes exhibits a band of darkly stained cells. A similar structure was previously described in the *weaver* heterozygotes [23, 25]. However, as distinguished from these authors, current findings supply additional information regarding the degree of cellularity in each studied region. Furthermore, our results notice that the presence of this band of cells is independent of: (1) whether a concavity or convexity is considered. For example, it is found both in the deep of the fissure prima and in the top of the pyramis, (2) analyzed lobe. The band is detected both in the anterior and in the posterior lobes, and (3) the neurogenetic timetables of GCs. This is so because the band of cells is observed both in the lingula and in the tuber, two lobules whose GCs have different times of origin [1]. Lastly, we provide evidence that this band is not present in the *weaver* heterozygotes tagged as $+/wv^0$ or +/+ sub-phenotypes.

The identity of the cells constituting the band cannot be unequivocally ascertained from our results. However, judging by shape and size of their nuclei, and cytoplasms, we suggest that most of them are young GCs. Moreover, after carefully analyzing sections, it is also proposed that these microneurons are arrested in the ML. This is based on a number of lines of evidence: (1) the rate of GCs migration is slower in the *weaver* heterozygous than in the +/+ but superior to the *wv*/*wv* GCs [23], (2) tissue culture experiments from postnatal cerebella reported impairments in the migratory behavior of +/*wv* GCs [49, 50], and (3) $+/wv \leftrightarrow +/+$ chimeras demonstrated that the migratory defect in the +/*wv* GCs is a defect that is to the GCs themselves [33].

Results obtained in the wv^0/wv^2 denote that at the level of the culmen, both the outer proliferative layer and the inner

Table 9 Spatial disposition of Purkinje cells and cellular density in the molecular layer of the +/wv^1 and +/wv^2 phenotypes

Area	Arrangement of PCs		Density of cells in the ML	
	+/wv^1	+/wv^2	+/wv^1	+/wv^2
Lingula	×	×	++	+++
Culmen	×	×	+++	++
Centralis	×	××	++	++
Tuber	××	××	+++	+++
Pyramis	××	××	+++	+++
Uvula	××	×	++	++
Nodulus	×	××	++	+
F. prima	××	×××	+++	+++
F. secunda	××	××	++	++
F. posterolateralis	×	××	++	+

The arrangement of PCs was considered from × (a quasimonolayer) to ××× (PCs located in three strata)

Density of cells in the ML was considered from + (scattered cells, although in a higher density than those in the wild-type phenotype) to +++ (hypercellular)

premigratory layer of the EGL exhibit a severe depletion of cells. It is presumed that the same occurs in the remainder studied areas, but, in accordance with our observations, the loss of cells is less intense. As the proliferative layer is disturbed, an important number of GCs are never generated because their precursors die. The decrease in the length of the cerebellar cortex, as well as in the EGL area, observed in the present paper may be related to the loss of GCs precursors. On this matter, it has been documented that the selective elimination of GCs precursors with X-irradiation [1], DNA-modifying agents [51], hyperthyroidism [52] or cytostatic drugs [53] produce a miniaturization of the cerebellum. At the present, it is unknown why GCs precursors are lost. Previous cell ablation experiments [46] and studies of mutant chimeric mice [54, 55] indicate a powerful influence of PCs on the mitotic activity of these neuroblasts.

In addition to the depletion of GCs precursors, we know from the literature that GCs are lost both in the +/*wv* and *wv*/*wv* vermis due to a direct effect of the mutated gene [8, 30, 33, 56]. Two models for GCs death have been proposed [57]. The first claims that continuous depolarization, due to the constitutively active GIRK2*wv* channel, results in elevated intracellular Ca^{2+} levels which lead to cells death. The second states that the loss of GIRK2 channel function reduces a major inhibitory pathway in developing neurons, resulting in GC hyperexcitability and causing cell death. Reductions in the ML area observed in the present paper may be related to a lesser density of parallel fibers as a consequence of GCs deficiency.

The deficit of PCs found in this work is in accordance with previous reports [23–27]. How the expression of the

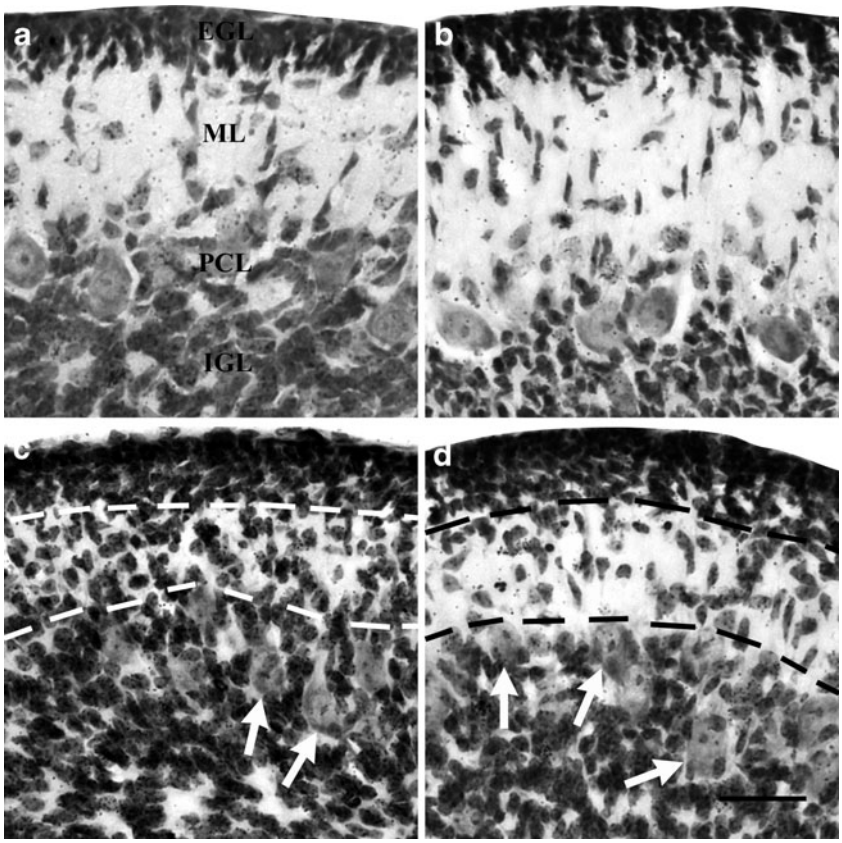

Fig. 5 High magnification photomicrographs of sagittal sections from +/+ (**a**–**b**) and +/w^1 (**c**–**d**). Photomicrographs **a** and **c** correspond to the fissure prima, and **b** and **d** to the uvula. *egl* External germinal layer, *ml* molecular layer, *pcl* Purkinje cell layer, *igl* internal granular layer. *Arrows* show examples of Purkinje cells. *Dashed lines* delimit the molecular layer in which a band of darkly stained cells is observed. *Scale bar* 25 μm

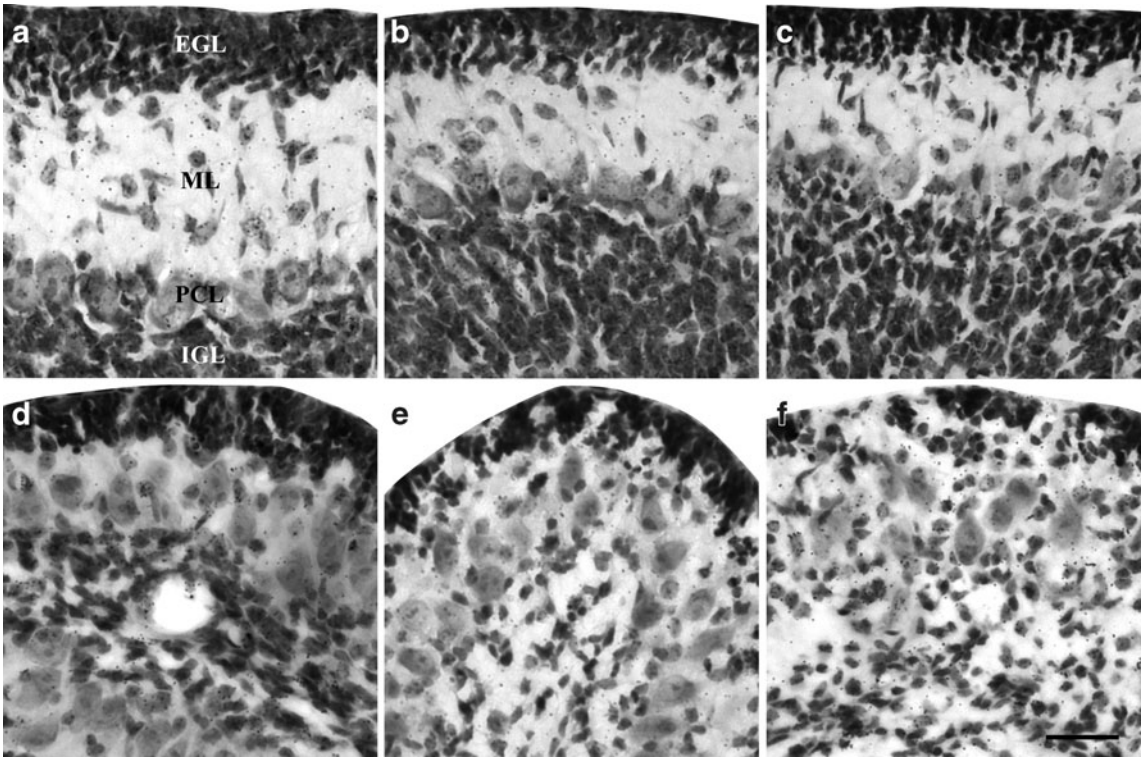

Fig. 6 High magnification photomicrographs of sagittal sections from +/+ (**a**–**c**) and wv^0/wv^2 (**d**–**f**). Photomicrographs **a** and **d** correspond to the lingula, **b** and **e** to the centralis and **c** and **f** to the culmen. *egl* External germinal layer, *ml* molecular layer, *pcl* Purkinje cell layer, *igl* internal granular layer. *Scale bar* 25 μm

weaver gene affects to these macroneurons remains unknown. An attractive hypothesis proposes that one of the aspects of the *weaver* sub-phenotype is a failure of the cell movements that lead to the fusion of the initially separate bilateral cerebellar anlage, and that this failure to migrate properly leaves some PCs in a position where they are unable to make appropriate connections, leading to their death [27, 28].

In contrast to the wild type, the mutant sub-phenotypes described in the present paper have their foliar patterns altered. Impairments are much more evident in the sub-phenotypes with two doses of the *weaver* gene (wv^0/wv^1 and wv^0/wv^2) than in those presenting only one ($+/wv^0$, $+/wv^1$ and $+/wv^2$). From these results, the subsequent question is which factors are behind the altered foliation observed when the *weaver* mutation is present? Nowadays, this is a mystery. In the discussion that follows, we relate GCs, their precursors and PCs as key elements of this enigma. Moreover, in order to propose a model of the *weaver* gene action on the fissuration pattern, one should go back to the prenatal life to understand what happen at P8.

Table 10 Variation in the EGL cells number per section in three lobules of the anterior lobe

Lobules	Phenotype	
	+/+	wv^0/wv^2
Lingula	1,250±48.5	312.5±15[a] (25 %)
Centralis	1,186±44.1	201.6±11[a] (17 %)
Culmen	1,203±39.5	96.2±7[a]* (8 %)

Values are expressed as mean±SEM

Numbers in parentheses indicate percentages in relation to +/+ animals

[a] Means are statistically different (see text)

Earlier research reported that, in normal rodent cerebellum, the smooth cerebellar primordium is divided, at E18.5, by the three principle fissures to generate the four cardinal lobes [1]. Most hypotheses of the cerebellar foliation point to the likely role of mechanical stresses arising from the production of GCs [1, 52, 58]. We have evidences that, around E19, GCs progenitors and PCs loss was detectable in the cerebellar vermis of the *weaver* homozygotes [59]. The same study also demonstrated that, in mutant embryos, the thickness of EGL and cardinal fissures were smaller in comparison to +/+. Heterozygous *weaver* affectation was in between +/+ and *wv*/*wv*.

As the +/+ cerebellum develops, cardinal fissures grow and lobes are divided into lobules. At P8, most lobules are observed and sublobules have begun to form (Fig. 4a). By contrast, the fissure that determines the limit between the declive and the folium is not present either in those *weaver* heterozygotes cataloged as $+/wv^1$ or in the wv^0/wv^1 and

wv^0/wv^2 sub-phenotypes (Fig. 4c, e, f). Moreover, in the sub-phenotypes $+/wv^0$, $+/wv^1$ and $+/wv^2$, the centralis is not divided in sublobules (Fig. 4b–d). The same occurs in the wv^0/wv^1 and wv^0/wv^2 sub-phenotypes, which in addition showed the culmen undivided.

From these observations, it is proposed that the reduced foliar pattern observed in our sub-phenotypes might be due to the depletion of GCs precursors and PCs in the prenatal life. We know that in normal mice, the pattern of lobules is regulated after PCs are born [60] and these macroneurons are produced from embryonic days 10 to 14 [39, 42]. When the five sub-phenotypes detected were considered together and were compared to +/+, a consistent pattern emerged. In the sub-phenotype containing more PCs ($+/wv^0$), the rate of GCs precursor proliferation is higher and more GCs are produced. This sub-phenotype produces a less affected foliar pattern. The $+/wv^2$ sub-phenotype, on the other hand, presents less PCs and in consequence less GCs are generated because GCs precursor proliferation is lower. The foliar pattern is more affected. Lastly, the wv^0/wv^2 exhibits lesser PCs and, therefore, GCs precursor proliferation is lowest. In consequence the foliar pattern is very affected.

In addition to the possible involvement of GCs proliferation and PCs, it cannot be ruled out that other genes implicated in the cerebellar foliation may be affected by the *weaver* gene expression [61]. This is because, in our colony, the *weaver* mutation is maintained by repeated crossing of carrier animals to a C57BL/6 X CBA F1 hybrid mate, and intercrossing of the progeny to generate litters segregating *wv*/*wv* homozygotes. These litters will also segregate all other genetic loci at which the C57BL/6 and CBA strains carry different alleles. This uncontrolled and undefined genetic variability may be a factor involved in the sub-phenotypic differences observed. In the future, experiments can be designed to identify gene expression differences that correlate with the sub-phenotypes reported here.

Further work on the *weaver* mutant may shed new light on how this mutation impairs the cytoarchitecture of the cerebellar cortex, and may be an excellent animal model for studying mechanisms involved in the cerebellar foliation.

Conclusion

The coexistence of several sub-phenotypes in the *weaver* mutant is reported for the first time and they have been reliably categorized by PCA-based cluster analysis of several morphological parameters from the cerebellar cortex.

Acknowledgments The authors are very grateful to Dr. Shirley A. Bayer for providing *weaver* mice. This research was supported by grants, FIS10-00975, FMM-08, SGR2009-00761.

References

1. Altman J, Bayer SA. Development of the cerebellar system. In: Relation to its evolution, structure and functions. Boca Raton: CRC Press; 1997.
2. Sultan F, Glickstein M. The cerebellum: comparative and animal studies. Cerebellum. 2007;6(3):168–76.
3. Armstrong DM, Schild RF. An investigation of the cerebellar corticonuclear projections in the rat using an autoradiographic tracing method. II. Projections from the hemisphere. Brain Res. 1978;141(2):235–49.
4. Cholley B, Wassef M, Arsenio-Nunes L, Brehier A, Sotelo C. Proximal trajectory of the brachium conjunctivum in rat fetuses and its early association with the parabrachial nucleus. A study combining in vitro HRP anterograde axonal tracing and immunocytochemistry. Brain Res Dev Brain Res. 1989;45(2):185–202.
5. Teune TM, van der Burg J, van der Moer J, Voogd J, Ruigrok TJ. Topography of cerebellar nuclear projections to the brain stem in the rat. Prog Brain Res. 2000;124:141–72.
6. Schilling K, Oberdick J, Rossi F, Baader SL. Besides Purkinje cells and granule neurons: an appraisal of the cell biology of the interneurons of the cerebellar cortex. Histochem Cell Biol. 2008;130(4):601–15.
7. Chedotal A. Should I, stay or should I go? Becoming a granule cell. Trends Neurosci. 2010;33(4):163–72.
8. Sotelo C, Changeux JP. Bergmann fibers and granular cell migration in the cerebellum of homozygous weaver mutant mouse. Brain Res. 1974;77(3):484–91.
9. Sato T, Joyner AL, Nakamura H. How does Fgf signaling from the isthmic organizer induce midbrain and cerebellum development? Dev Growth Differ. 2004;46(6):487–94.
10. Nakamura H, Sato T, Suzuki-Hirano A. Isthmus organizer for mesencephalon and metencephalon. Dev Growth Differ. 2008;50 Suppl 1:S113–8.
11. Suzuki-Hirano A, Harada H, Sato T, Nakamura H. Activation of Ras-ERK pathway by Fgf8 and its downregulation by Sprouty2 for the isthmus organizing activity. Dev Biol. 2010;337(2):284–93.
12. Leto K, Carletti B, Williams IM, Magrassi L, Rossi F. Different types of cerebellar GABAergic interneurons originate from a common pool of multipotent progenitor cells. J Neurosci. 2006;26(45):11682–94.
13. Carletti B, Rossi F. Neurogenesis in the cerebellum. Neuroscientist. 2008;14(1):91–100.
14. Reeves RH, Crowley MR, Lorenzon N, Pavan WJ, Smeyne RJ, Goldowitz D. The mouse neurological mutant weaver maps within the region of chromosome 16 that is homologous to human chromosome 21. Genomics. 1989;5(3):522–6.
15. Mjaatvedt AE, Citron MP, Reeves RH. High-resolution mapping of D16led-1, Gart, Gas-4, Cbr, Pcp-4, and Erg on distal mouse chromosome 16. Genomics. 1993;17(2):382–6.
16. Patil N, Cox DR, Bhat D, Faham M, Myers RM, Peterson AS. A potassium channel mutation in weaver mice implicates membrane excitability in granule cell differentiation. Nat Genet. 1995;11(2):126–9.
17. Tolwani RJ, Jakowec MW, Petzinger GM, Green S, Waggie K. Experimental models of Parkinson's disease: insights from many models. Lab Anim Sci. 1999;49(4):363–71.
18. Triarhou LC. Biology and pathology of the Weaver mutant mouse. Adv Exp Med Biol. 2002;517:15–42.
19. Grusser-Cornehls U, Baurle J. Mutant mice as a model for cerebellar ataxia. Prog Neurobiol. 2001;63(5):489–540.
20. Lalonde R, Strazielle C. Spontaneous and induced mouse mutations with cerebellar dysfunctions: behavior and neurochemistry. Brain Res. 2007;1140:51–74.
21. Triarhou LC, Norton J, Ghetti B. Mesencephalic dopamine cell deficit involves areas A8, A9 and A10 in weaver mutant mice. Exp Brain Res. 1988;70(2):256–65.

22. Cavalcanti-Kwiatkoski R, Raisman-Vozari R, Ginestet L, Del Bel E. Altered expression of neuronal nitric oxide synthase in weaver mutant mice. Brain Res. 2010;1326:40–50.
23. Rezai Z, Yoon CH. Abnormal rate of granule cell migration in the cerebellum of "Weaver" mutant mice. Dev Biol. 1972;29(1):17–26.
24. Rakic P, Sidman RL. Organization of cerebellar cortex secondary to deficit of granule cells in weaver mutant mice. J Comp Neurol. 1973;152(2):133–61.
25. Rakic P, Sidman RL. Sequence of developmental abnormalities leading to granule cell deficit in cerebellar cortex of weaver mutant mice. J Comp Neurol. 1973;152(2):103–32.
26. Blatt GJ, Eisenman LM. A qualitative and quantitative light microscopic study of the inferior olivary complex of normal, reeler, and weaver mutant mice. J Comp Neurol. 1985;232(1):117–28.
27. Herrup K, Trenkner E. Regional differences in cytoarchitecture of the weaver cerebellum suggest a new model for weaver gene action. Neuroscience. 1987;23(3):871–85.
28. Maricich SM, Soha J, Trenkner E, Herrup K. Failed cell migration and death of purkinje cells and deep nuclear neurons in the weaver cerebellum. J Neurosci. 1997;17(10):3675–83.
29. Marti J, Wills KV, Ghetti B, Bayer SA. Evidence that the loss of Purkinje cells and deep cerebellar nuclei neurons in homozygous weaver is not related to neurogenetic patterns. Int J Dev Neurosci. 2001;19(6):599–610.
30. Won L, Ghetti B, Heller B, Heller A. In vitro evidence that the reduction in mesencephalic dopaminergic neurons in the weaver heterozygote is not due to a failure in target cell interaction. Exp Brain Res. 1997;115(1):174–9.
31. Hess EJ. Identification of the weaver mouse mutation: the end of the beginning. Neuron. 1996;16(6):1073–6.
32. Eisenman LM, Gallagher E, Hawkes R. Regionalization defects in the weaver mouse cerebellum. J Comp Neurol. 1998;394(4):431–44.
33. Goldowitz D, Mullen RJ. Granule cell as a site of gene action in the weaver mouse cerebellum: evidence from heterozygous mutant chimeras. J Neurosci. 1982;2(10):1474–85.
34. Armstrong C, Hawkes R. Selective Purkinje cell ectopia in the cerebellum of the weaver mouse. J Comp Neurol. 2001;439(2):151–61.
35. Ward Jr JH. Hierarchical grouping to optimize an objective function. J Am Stat Assoc. 1963;58(301):236–44.
36. Kshirsagar AM. Multivariate analysis. New York: Dekker; 1972.
37. Anderberg MR. Cluster analysis for applications. New York: Academic Press; 1973.
38. Benavides-Piccione R, Hamzei-Sichani F, Ballesteros-Yanez I, DeFelipe J, Yuste R. Dendritic size of pyramidal neurons differs among mouse cortical regions. Cereb Cortex. 2006;16(7):990–1001.
39. Marti J, Carmen Santa-Cruz M, Bayer SA, Hervas JP. The weaver gene expression affects neuronal generation patterns depending on age and encephalic region. Neurosci Lett. 2006;396(3):202–6.
40. Wei J, Hodes ME, Wang Y, Feng Y, Ghetti B, Dlouhy SR. Direct cDNA selection with DNA microdissected from mouse chromosome 16: isolation of novel clones and construction of a partial transcription map of the C3-C4 region. Genome Res. 1996;6(8):678–87.
41. Lange W (1982) Regional differences in the cytoarchitecture of the cerebellar cortex. Palay SL, Chan-Palay V (eds). The cerebellum: new vistas. Springer: Berlin. pp 93–107
42. Marti J, Santa-Cruz MC, Bayer SA, Ghetti B, Hervas JP. Purkinje cell age-distribution in fissures and in foliar crowns: a comparative study in the weaver cerebellum. Brain Struct Funct. 2007;212(3–4):347–57.
43. Sarle WS. Cubic clustering criterion. Technical report, Cary, NC: SAS Institute Inc 1983;A-108.
44. Hartigan JA. Clustering algorithms. New York: Wiley; 1975.
45. Inouye M, Murakami U. Temporal and spatial patterns of Purkinje cell formation in the mouse cerebellum. J Comp Neurol. 1980;194(3):499–503.
46. Smeyne RJ, Goldowitz D. Development and death of external granular layer cells in the weaver mouse cerebellum: a quantitative study. J Neurosci. 1989;9(5):1608–20.
47. Simon JR, Ghetti B. The weaver mutant mouse as a model of nigrostriatal dysfunction. Mol Neurobiol. 1994;9(1–3):183–9.
48. Harrison SM, Roffler-Tarlov SK. Cell death during development of testis and cerebellum in the mutant mouse weaver. Dev Biol. 1998;195(2):174–86.
49. Willinger M, Margolis DM. Effect of the weaver (wv) mutation on cerebellar neuron differentiation. I. Qualitative observations of neuron behavior in culture. Dev Biol. 1985;107(1):156–72.
50. Willinger M, Margolis DM. Effect of the weaver (wv) mutation on cerebellar neuron differentiation. II. Quantitation of neuron behavior in culture. Dev Biol. 1985;107(1):173–9.
51. Doughty ML, Delhaye-Bouchaud N, Mariani J. Quantitative analysis of cerebellar lobulation in normal and agranular rats. J Comp Neurol. 1998;399(3):306–20.
52. Lauder JM, Altman J, Krebs H. Some mechanisms of cerebellar foliation: effects of early hypo- and hyperthyroidism. Brain Res. 1974;76(1):33–40.
53. Pisu MB, Roda E, Guioli S, Avella D, Bottone MG, Bernocchi G. Proliferation and migration of granule cells in the developing rat cerebellum: cisplatin effects. Anat Rec A: Discov Mol Cell Evol Biol. 2005;287(2):1226–35.
54. Sonmez E, Herrup K. Role of staggerer gene in determining cell number in cerebellar cortex. II. Granule cell death and persistence of the external granule cell layer in young mouse chimeras. Brain Res. 1984;314(2):271–83.
55. Hamre KM, Goldowitz D. Analysis of gene action in the meander tail mutant mouse: examination of cerebellar phenotype and mitotic activity of granule cell neuroblasts. J Comp Neurol. 1996;368(2):304–15.
56. Hatten ME, Liem RK, Mason CA. Weaver mouse cerebellar granule neurons fail to migrate on wild-type astroglial processes in vitro. J Neurosci. 1986;6(9):2676–83.
57. Harkins AB, Fox AP. Cell death in weaver mouse cerebellum. Cerebellum. 2002;1(3):201–6.
58. Mares V, Lodin Z. The cellular kinetics of the developing mouse cerebellum. II. The function of the external granular layer in the process of gyrification. Brain Res. 1970;23(3):343–52.
59. Bayer SA, Wills KV, Wei J, Feng Y, Dlouhy SR, Hodes ME, et al. Phenotypic effects of the weaver gene are evident in the embryonic cerebellum but not in the ventral midbrain. Brain Res Dev Brain Res. 1996;96(1–2):130–7.
60. Cheng Y, Sudarov A, Szulc KU, Sgaier SK, Stephen D, Turnbull DH, et al. The engrailed homeobox genes determine the different foliation patterns in the vermis and hemispheres of the mammalian cerebellum. Development. 2010;137(3):519–29.
61. Airey DC, Lu L, Williams RW. Genetic control of the mouse cerebellum: identification of quantitative trait loci modulating size and architecture. J Neurosci. 2001;21(14):5099–109.